SYNTHESIS AND CHARACTERIZATION OF A NOVEL LIGAND AND SPECTROSCOPIC STUDY OF THE FORMATION OF ITS COMPLEXES WITH DIFFERENT CATIONS AND THEIR SENSORY CHARACTERISTICS**

M. Shariati-Rad [1*], M. Karimi [1], M. Rezaeivala [2]

[1] Razi University, Department of Analytical Chemistry, Faculty of Chemistry, Kermanshah, Iran; e-mail: mshariati_rad@yahoo.com
[2] Hamedan University of Technology, Department of Chemical Engineering, Hamedan 65155, Iran

A new ligand (L), N,N'-bis(2-hydroxybenzyl)-1,2-diaminoethane, was synthesized and characterized. The sensing behavior of L toward various metal ions was investigated by spectrofluorometric and UV-Vis spectrophotometric methods. The sensor displayed selective and sensitive recognition toward Fe^{3+} and Fe^{2+} in acetonitrile. The fluorescence of L was quenched mainly by Fe^{3+}, and a considerable enhancement of fluorescence was observed in the presence of Zn^{2+}. Using multivariate hard modeling and stoichiometry, the concentration, spectral profiles, and formation constants of the studied complexes were calculated.

***Keywords*:** *spectrofluorometric, spectrophotometric, hard-modelling, formation constant.*

СИНТЕЗ И ИССЛЕДОВАНИЕ НОВОГО ЛИГАНДА. ИЗУЧЕНИЕ СПЕКТРОСКОПИЧЕСКИМИ МЕТОДАМИ ОБРАЗОВАНИЯ ЕГО КОМПЛЕКСОВ С РАЗЛИЧНЫМИ КАТИОНАМИ И ИХ СЕНСОРНЫХ СВОЙСТВ

M. Shariati-Rad [1*], M. Karimi [1], M. Rezaeivala [2]

УДК 543.42.062

[1] Университет Рази, Керманшах, Иран; e-mail: mshariati_rad@yahoo.com
[2] Хамаданский технологический университет, 65155, Хамадан, Иран

(Поступила 20 июня 2016)

Синтезирован и исследован лиганд (L) N,N'-бис(2-гидроксибензил)-1,2-диаминоэтан. С помощью спектрофлуориметрии и спектроскопии в ультрафиолетовом и видимом диапазонах изучена чувствительность L к ионам различных металлов. Сенсор на основе L обнаруживает высокую чувствительность в отношении ионов Fe^{3+} и Fe^{2+} в ацетонитриле. Тушение флуоресценции L обусловлено главным образом ионами Fe^{3+}, а ее значительное усиление наблюдается в присутствии ионов Zn^{2+}. С помощью многофакторного моделирования рассчитаны стехиометрия, концентрация и спектральные профили, а также константы образования изучаемых комплексов.

***Ключевые слова*:** *спектрофлуориметрическое и спектрофотометрическое моделирование, константа образования комплексных соединений.*

Introduction. A chemosensor is a molecule that significantly changes in electronic, magnetic, or optical properties when it binds to a specific guest counterpart. Among the various types of chemosensors, fluorescent chemosensors have several advantages due to their high sensitivity, intrinsic specificity, fast response, and real-time detection capabilities [1]. Fluorescent sensors have attracted much attention for the detection of metal ions, which has led to the development of highly specific probes with a broad range of applications in chemistry, biochemistry, and cell biology [2]. Fluorescent chemosensors for metal ions such as Fe^{3+} [3], Cu^{2+} [4], Zn^{2+} [5], Co^{2+} [6], Mg^{2+} [7], Hg^{2+} [8], Al^{3+} [9], and Pb^{2+} [10] have been reported.

** Full text is published in JAS V. 84, No. 6 (http://springer.com/10812) and in electronic version of ZhPS V. 84, No. 6 (http://www.elibrary.ru/title_about.asp?id=7318; sales@elibrary.ru).

On the other hand, colorimetric measurements are particularly promising, since they are simple and powerful methods, which depend on the visible color change, and there is thereby no need for spectroscopic devises [11]. There is an increasing interest in the development of a new generation of molecules for sensing chemical species in the environment. Among them, chromogenic receptors are especially attractive because the recognition process with their help is accomplished with an easy-to-detect perceptible color evolution. Recently, significant effort has been made to establish the theoretical basis for the chromogenic guest recognition. As a result, a number of selective chemosensors for anions, cations, and neutral species have been designed and synthesized [12, 13]. Compared with fluorescent and electrochemical sensors, colorimetric sensors have some obvious advantages, such as convenience, low cost, and good visualization [14].

Iron is one of the most essential elements for the normal physiological functioning of the human body. It plays an important role in many cellular processes, including DNA and RNA synthesis, energy generation, and oxygen transport [15, 16]. Iron deficiency can cause many diseases, such as anemia, liver damage, Parkinson's disease, intelligence decline, diabetes, and cancer [17–19]. If the iron concentration exceeds the normal level, it may become a potential health hazard. Excess amounts of iron in the body cause liver and kidney damage (hemochromatosis). Some iron compounds are suspected to be carcinogens. Hence, the need for the determination of iron ions in clinical, medicinal, environmental, and different industrial samples has resulted in a number of methods for its measurement [20–26]. However, it is necessary to design simple, highly sensitive, and selective chemosensors for the detection of different iron species and establish a method for the determination of trace amounts of these ions [27].

Zinc is an essential element, and it is the second most abundant transition metal after iron in the human body with a concentration ranging from sub-nmol/L to 0.3 mmol/L [28, 29]. Zn^{2+} plays many roles in numerous cellular functions, such as the regulation of gene expression, apoptosis, metalloenzyme catalysis, and neurotransmission in biological systems [30, 31]. Severe neurological diseases, such as Alzheimer's, cerebral ischemia and epilepsy [32–34], are associated with the disorder of Zn^{2+} metabolism. Therefore, the measurement of Zn^{2+} is of great importance in neurobiology. On the other hand, most of the reported fluorescent chemosensors for Zn^{2+} have encountered difficulty in distinguishing zinc from other transition metal ions [11, 35–37]. Consequently, the introduction of simple, highly selective, and efficient Zn^{2+} sensors remains of great interest.

In the present work, a new ligand is synthesized and characterized. Subsequently, its sensing ability toward different cations is studied. The formation constants of the complexes of the synthesized ligand with different cations were calculated using hard-modelling.

Theory of hard-modeling (HM). Data fitting is the calculation of a data set ($\mathbf{X}_{calc}$) that approximates the measured data. The calculated data set is defined by the chemical model and the parameters collected in the vector **k**. The measured data ($\mathbf{X}_{exp}$) minus the calculated one is the error matrix, **E**:

$$\mathbf{E} = \mathbf{X}_{exp} - \mathbf{X}_{calc}(\text{model}, \mathbf{k}). \quad (1)$$

The matrices have dimensions $n \times m$, where n is the number of spectra (or mole ratios) and m is the number of wavelengths. In HM, fitting means finding a unique set of parameters for which the calculated data ($\mathbf{X}_{calc}$) closely approximate the measured one ($\mathbf{X}_{exp}$). The quality of the fit can be seen by *ssq*, which is the sum over the squares of all the elements of the matrix **E**:

$$ssq = \sum_{i=1}^{n}\sum_{j=1}^{m} E_{ij}^2 . \quad (2)$$

The above equations indicate that *ssq* is a function of the parameters, the model and the data. The chemical model and the parameters allow the computation of concentrations of all species as a function of the titration. This is done by the Newton–Raphson algorithm, as described elsewhere [38, 39]. The calculated concentrations for all components in all mole ratios are collected in the matrix **C**.

According to Beer–Lambert's law, the relationship between the concentrations (collected in the matrix **C**) and the measurements ($\mathbf{X}_{exp}$) can be expressed as a matrix equation:

$$\mathbf{X}_{exp} = \mathbf{C} \times \mathbf{S}^T + \mathbf{E} = \mathbf{X}_{calc} + \mathbf{E}. \quad (3)$$

The molar absorptivities of all species in the studied wavelength range are collected in the matrix $\mathbf{S}^T$ of dimensions $nc \times m$, and the dimension of the matrix **C** is $n \times nc$, where nc denotes the number of components. In HM, nc is the number of either absorbing or nonabsorbing species contributing to the model.

The parameters describing the chemical model are collected in the vector **k** in Eq. (1). The matrix $\mathbf{S}^T$ of molar absorptivities that relates the concentrations to the measured data contains linear parameters. The calculation of the nonlinear parameters **k** (formation constants) requires an iterative algorithm (Newton–

Raphson algorithm) that starts with initial guesses of the parameters. The algorithm converges towards the optimal solution in a reasonable number of iterations. Given $\mathbf{X}_{exp}$ and $\mathbf{C}$, the best estimate for $\mathbf{S}^T$ can be calculated explicitly as

$$\mathbf{S}^T = \mathbf{C}^+ \times \mathbf{X}_{exp}, \quad (4)$$

where $\mathbf{C}^+$ is the pseudo-inverse of $\mathbf{C}$ ($\mathbf{C}^+ = (\mathbf{C}^T \times \mathbf{C})^{-1} \times \mathbf{C}^T$). Therefore, $\mathbf{k}$ in Eq. (1) contains only the nonlinear parameters, and the linear ones are effectively eliminated by:

$$\mathbf{E} = \mathbf{X}_{exp} - \mathbf{C} \times \mathbf{S}^T = \mathbf{X}_{exp} - \mathbf{C} \times \mathbf{C}^+ \times \mathbf{X}_{exp}. \quad (5)$$

The equilibrium constants, which define the matrix $\mathbf{C}$, are refined to minimize the sum of squares of the matrix of residuals, *ssq*.

Experiment. All chemicals and solvents were of analytical reagent grade, purchased from Merck (Darmstadt, Germany) and used without further purification. Acetonitrile (AN) was employed to prepare all solutions. Stock solutions (1.0 mmol/L) of Al^{3+}, Co^{2+}, Pb^{2+}, Cd^{2+}, Hg^{+}, Ba^{2+}, Zn^{2+}, Ag^{+}, Ni^{2+}, Cu^{2+}, and Ca^{2+} were prepared by direct dissolution of proper amounts of the corresponding nitrate salts in acetonitrile. For the preparation of the corresponding solutions of Fe^{2+}, Fe^{3+}, Mg^{2+}, and Sr^{2+}, chloride salts were used.

UV-Vis absorption spectra were recorded by an Agilent UV-Vis 8453 spectrophotometer. Fluorescence spectra were recorded by a Jasco FP-6200 spectrofluorimeter with the excitation wave at 270 nm, while emission spectra were recorded in the wavelength range 280–800 nm.

The general method for the synthesis of the ligand *N*,*N*′-bis(2-hydroxybenzyl)-1,2-diaminoethane is as follows. A solution containing 20 mmol of ethane-1,2-diamine in dry ethanol (30 mL) was added dropwise to a warm solution of salicylaldehyde (4.88 g, 40 mmol) in dry ethanol (30 mL) during 2 h. The mixture was refluxed under stirring for 12 h and then allowed to cool to room temperature. Solid sodium borohydride (6.05 g, 160 mmol) was then added slowly, and the reaction mixture was heated at reflux for a further 2 h. The solution was filtered, and the volume of the filtrate was reduced to 20 mL by rotary evaporation. Excess water was added, and the product was extracted by chloroform (3×25 mL). The combined chloroform solutions were separated and dried over magnesium sulfate. Chloroform was removed by rotary evaporation, leaving the product. Analytical calculations for $C_{16}H_{20}N_2O_2$ (MW: 272.15): C 70.56%; H 7.40%; N 10.29%. Found: C 70.86%; H 7.32%; N 10.32%. Yield: 90%. Melting point: 119–121°C. FTIR (KBr, cm^{-1}): 3309 [υ(N-H)], 1601 [υ(C=C)], 1591. ^{1}H NMR (400 MHz, $CDCl_3$, ppm) δH: 6.97 (dd, 2H, H-3), 6.78 (dt, 2H, H-4), 7.19 (dt, 2H, H-5), 6.83 (dd, 2H, H-6), 4.00 (s, 4H, $PhCH_2N$), 2.85 (s, 4H, $N\text{-}CH_2CH_2$). ^{13}C NMR (400 MHz, $CDCl_3$, ppm) δC: 158.2 (C-1), 122.4 (C-2), 128.7 (C-3), 116.7 (C-4), 129.1 (C-5), 119.5 (C-6), 52.9 (C-7), 48.1 (C-8). The structural formula of the synthesized ligand is

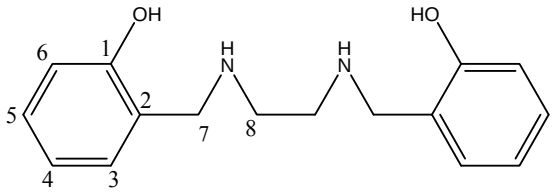

Procedure for the study of the complex formation using the mole ratio. Stock solutions of the metal ions (1.0 mmol/L) were prepared in AN, and a stock solution of L (100.0 μmol/L) was prepared in AN and stored in the dark. The solution of L was then diluted to 40 μmol/L with AN. In titration experiments, 2.5 mL of the resulting solution of L was placed in a quartz cell and titrated with different volumes of the concentrated metal ion added by a micro-syringe, and, immediately, absorption or fluorescence spectra were recorded. All the measurements were made at 25ºC (±0.1).

Results and discussion. The tetradentate amine, ***N***,*N*′-bis(2-hydroxybenzyl)-1,2-diaminoethane, was prepared in 90% yield. The ^{1}H and ^{13}C NMR spectra of L indicate that this compound has been successfully synthesized.

UV-Vis absorption spectra. The absorption spectrum of L in AN shows an absorption band at 275 nm, which can be attributed to the $\pi \rightarrow \pi^*$ aromatic system transition. Fe^{3+}, Fe^{2+}, Mg^{2+}, Cu^{2+}, and Co^{2+} produced color changes after their addition to a solution containing L. However, the color change is more distinct for Fe^{3+} and Fe^{2+} ions. The color of L in the presence of different cations is shown in Fig. 1. As can be seen, in the presence of iron species, the color changes are more pronounced and distinct. For a large number of cations, including Na^{+}, K^{+}, Ca^{2+}, Sr^{2+}, Ba^{2+}, Pb^{2+}, Al^{3+}, Ni^{2+}, Hg^{+}, Hg^{2+}, Cd^{2+}, Zn^{2+}, and Ag^{+}, no color change in the solution of L after the addition of cations was observed.

The sequential addition of L to the solution containing Fe^{3+} in mole ratios 0–3 results in the gradual increase of the intensity of the Fe^{3+} bands at 240, 277, 315, and 360 nm. This change is more pronounced for the band at 240 nm. For further exploration, this equilibrium was studied by adding Fe^{3+} to L in mole ratios 0–3. The variations in the absorption spectra are shown in Fig. 2. As can be seen, up to the mole ratio of about 1, the intensities of the bands at 277 (belong to L) and 315 nm (a new band) increase gradually. By continuing the titration beyond the mole ratio of 1, a new band at 360 nm appeared. These changes can be seen up to the mole ratio of 3. Moreover, a less intense band located at 486 nm can be seen during the addition of Fe^{3+} to L.

After the addition of different cations to the solution containing L with a concentration of 100.0 μmol/L, UV-Vis spectra were recorded. The resulted spectra are shown in Fig. 3. These spectra signify the colors shown in Fig. 1. As can be seen from Fig. 3, the variation in the spectrum of L in the presence of Fe^{2+} and Fe^{3+} is more pronounced and covers a wavelength region distinct from the other cations.

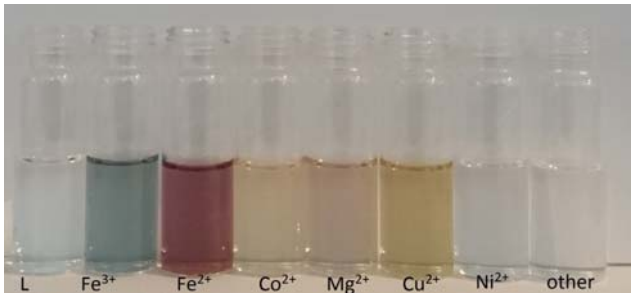

Fig. 1. The color change of L (100 μmol/L) upon addition of various metal ions (10 equiv).

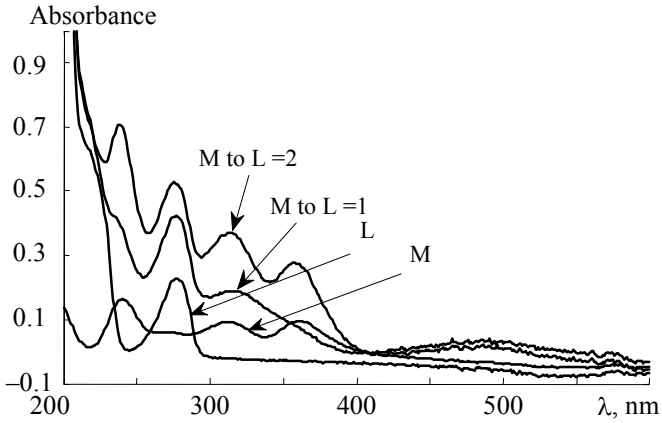

Fig. 2. Spectra of the Fe^{3+} (M) and the ligand (L) with concentrations of 100.0 μmol/L, and spectra of mixtures in 1:1 and 2:1 mole ratios.

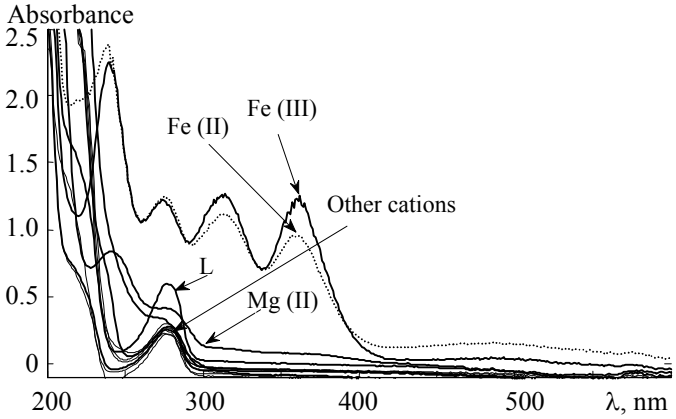

Fig. 3. Absorption spectra of L (100.0 μmol/L) in the presence of 10 equivalents of different metal ions.

Fluorescence spectra. The fluorescence spectrum of L in the presence of different cations in different mole ratios can be seen in Fig. 4. The fluorescence spectra have maxima at about 300 and 600 nm. A sharp peak located at about 540 nm can also be observed in the spectra, which can be related to the blank (solvent). As can be seen from Fig. 4a, after the addition of M to the solution of L, the fluorescence intensity increases up to the mole ratio of 1:1. This increase is more pronounced for Zn^{2+} (about twice of Fe^{2+}) and Fe^{2+}. Upon complexation with Zn^{2+}, the intramolecular photo electron transfer (PET), which results in quenching, could be decreased by reducing the electron density of lone pairs through metal–donor binding interaction, which results in the increased ligand emission. In contrast, the fluorescence quenching was observed in higher mole ratios. By continuing addition of M to L beyond the mole ratio of 1:1, a decrease in the fluorescence intensity for all cations except for Al^{3+} and Mg^{2+} can be observed (see Fig. 4b). The observed fluorescent enhancement can be attributed to the formation of a rigid system after binding with these cations. Al^{3+} weakly affects the fluorescence intensity of L. The quenching effect in the mole ratio of 3:1 and higher can be seen for Fe^{3+} (see Fig. 4b). The quenching can be due to the very fast and efficient nonradiative decay of the excited states resulting from the electron or energy transfer between the open shell *d*-orbital of the metal ion and the ligand [40, 41]. In the case of Fe^{3+}, the gradual quenching of fluorescence is accompanied by a small red shift (4 nm). Paramagnetic fluorescence quenching may be invoked to explain the fluorescence spectral behavior of L in the presence of Fe^{3+}. In the close proximity of the paramagnetic metal ion and the fluorophore, the intersystem crossing (isc) phenomenon is promoted. The subsequent loss of energy from the S_1 to T_1 state of the fluorophore usually occurs via bimolecular nonradiative processes resulting in paramagnetic fluorescence quenching. Due to the paramagnetic nature of the ferric ion, most of the reported sensors for Fe^{3+} are based on fluorescence quenching mechanisms [42–44].

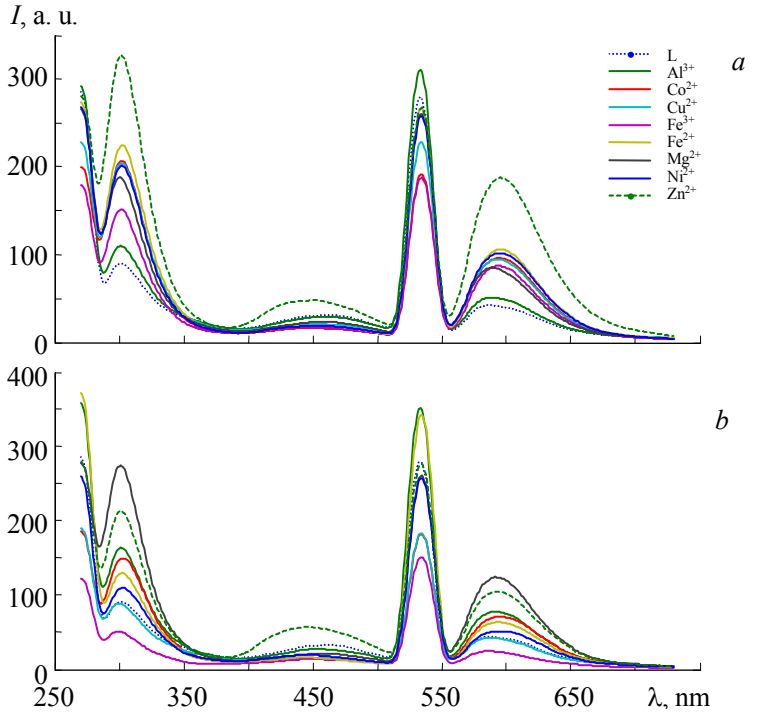

Fig. 4. Spectrum of L (100 μmol/L) in the presence of different cations in mole ratio (M to L) of (a) 1:1 and (b) 3:1. Excitation wavelength is 270 nm.

UV-Visible spectrophotometric titrations. In order to study the complex formation of L with different cations, the mole ratio method was employed. The variation in the absorbance of L in the presence of increasing amounts of cations was recorded. Typical recorded data are shown in Fig. 5. The main absorption peak of L is located at 270 nm. However, L absorbs in the range 200–240 nm. In all cases, after the addition of cation, an increase in the intensity of the absorption bands of L is observed. However, especially in the presence of Fe^{3+} and Fe^{2+}, new absorption peaks beyond 300 nm appear. For Fe^{3+}, new peaks at 240, 315, and 360 nm are observed. For Fe^{2+}, the new peak is observed at 320 and about 545 nm.

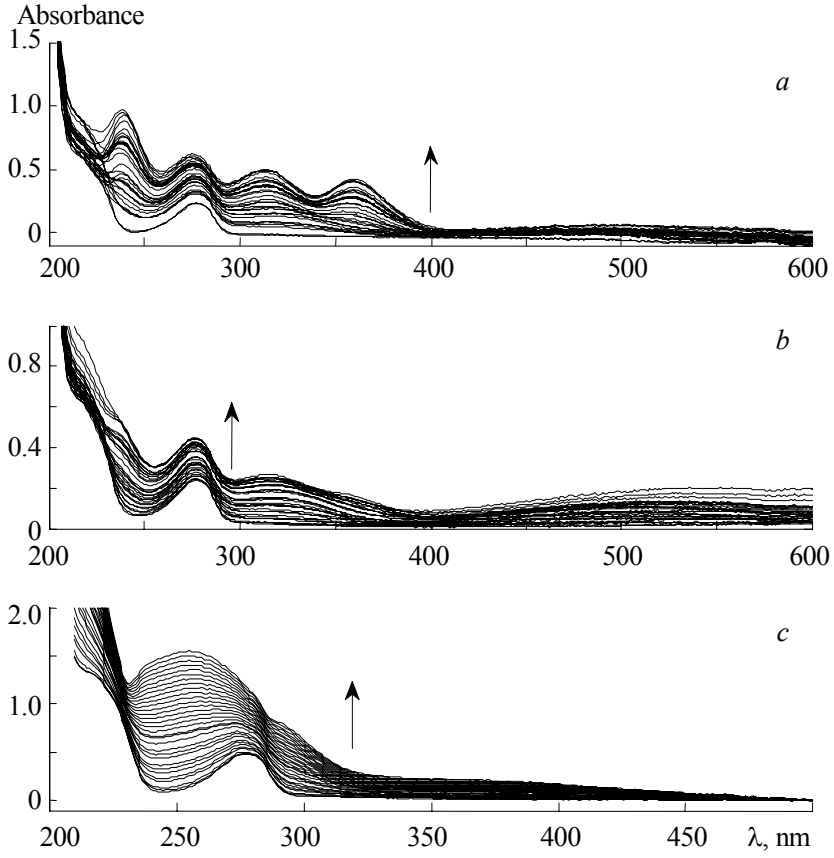

Fig. 5. Spectral changes during addition of (a) Fe^{3+}, (b) Fe^{2+}, and (c) Co^{2+} to a solution containing L (100.0 μmol/L) in mole ratio of 0–3.

Determination of the formation constant of complexes by HM. In the next step, for the evaluation of the stability of different complexes, hard-modeling was used [45–47]. All the calculations were performed in MATLAB. The common Newton–Raphson algorithm was used for the nonlinear hard-modeling by a series of functions written as *m*-files in the MATLAB environment.

Generally, HM approaches have excellent performance if the equilibrium model is appropriately set and if all the variation related to the spectrometric response is linked to the components involved in the process. A model is a function that describes the matrix **C** of the concentrations of all the components in the system. Modeling the process under investigation is the core of any HM algorithm. HM helps chemists to explain the measurements by using a chemical model and to determine the actual values of the parameters, i.e., absorptivity, the rate or equilibrium constants, etc. One of the advantages of HM is that intermediates, especially minor ones, are detected more reliably (in the absence of the linear dependency of the concentration profiles) and the identification of the unknown intermediates can be supported by the availability of their absorption spectra.

The calculated complex formation constants for different cations with L are reported in Table 1. The standard error of the stability constants is relatively low. This indicates that the models for performing HM were proposed appropriately and the calculated constants are reliable. The most stable complex of L with the ML formula is formed by Fe^{2+} and Fe^{3+}. For Cu^{2+}, the data did not fit the ML formula. It can be deduced that in the system of Cu^{2+} and L, such a complex does not exist. In the case of Zn^{2+}, no fit with the complexes ML and ML_2 was obtained. However, the model containing M_2L fits the data of the titration of L with Zn^{2+}. A different behavior of the system L-Zn^{2+} was also observed in the fluorescence study (a considerable increase in the fluorescence was observed after the addition of Zn^{2+} to L).

In the complex formation of Fe^{3+} and Fe^{2+} with L, the variation of the spectra and color was more evident. Therefore, two sets of data were acquired for these systems. In the first, a solution of L was titrated with M, and in the second, a solution of M was titrated by L. The data were simultaneously analyzed by HM considering two complexes ML and ML_2. The calculated profiles are shown in Fig. 6. The relatively low

TABLE 1. Calculated Formation Constants (K_f) by HM for Complexes of the Synthesized Ligand with Different Cations

Cation	logK_f	Standard error	*ssq*
Fe^{3+} (ML)	4.26	0.08	–
Fe^{3+} (ML_2)	7.48	0.10	17.67
Fe^{2+} (ML)	4.02	0.04	–
Fe^{2+} (ML_2)	6.76	0.03	8.29
Co^{2+} (ML)	3.34	0.14	0.33
Cu^{2+} (ML)	–	–	–
Cu^{2+} (ML_2)	5.74	0.03	1.02
Al^{3+} (ML)	1.69	0.35	5.76
Mg^{2+} (ML)	2.54	0.03	0.31
Ni^{2+} (ML)	1.72	0.12	1.32
Zn^{2+} (M_2L)	7.04	0.06	0.34

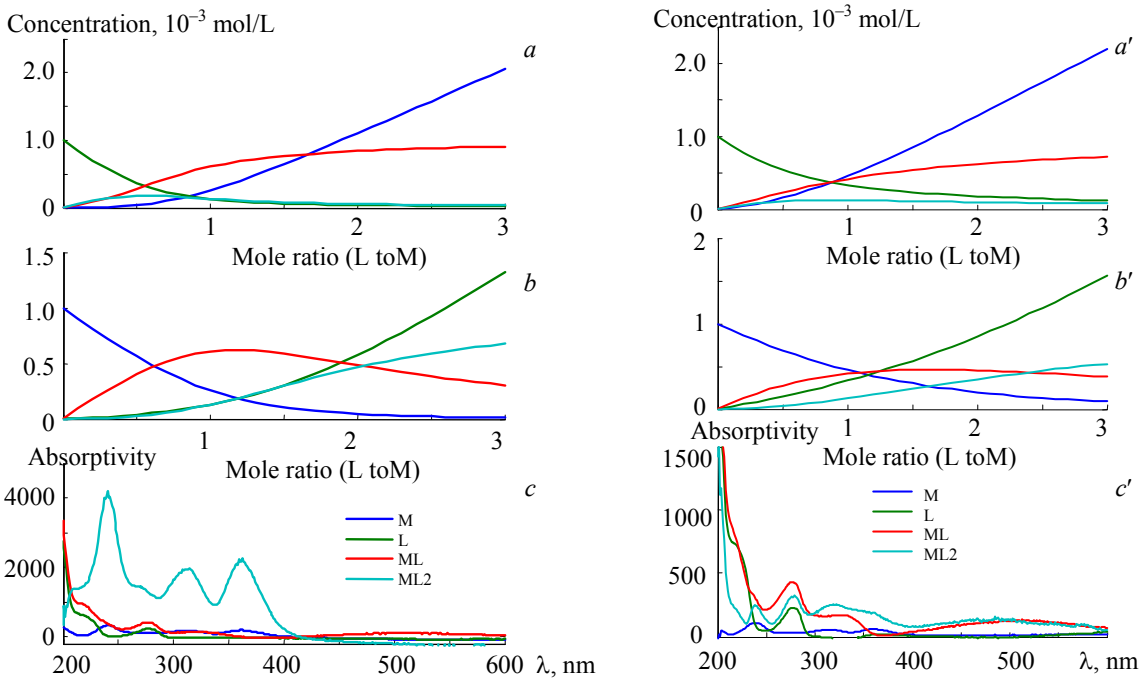

Fig. 6. Calculated concentration profiles for titration of L with M (a, a′), M with L (b, b′), and the calculated spectral profiles (c, c′). M is Fe^{3+} (a–c) and Fe^{2+} (a′–c′).

standard errors of the calculated formation constants for ML and ML_2 indicate that the model for M = Fe^{3+} and Fe^{2+} was conectly selected. The complex ML has spectral characteristics similar to L in the region 200–300 nm, especially when M = Fe^{3+} (Fig. 6c,c′). However, for ML, two broad peaks with maxima located at 320 and 520 nm (M = Fe^{3+}) (Fig. 6c) and at 340 and 500 nm (M = Fe^{2+}) (see Fig. 6c′) can be seen. The addition of L beyond the mole ratio of 1:1 causes the disappearance of the peak at 520 nm and the bifurcation of the band at 320 nm for the Fe^{3+}-L system. For the Fe^{2+}-L system, in these mole ratios, the band at 340 nm shifts to about 320 nm and now bears a shoulder at 360 nm. The spectral characteristics of ML_2 are very similar to that of M but with much greater intensity, especially for the peak located at 242 nm. With respect to the peaks at 313 and 360 nm for Fe^{3+}, which are of equal intensity, the peak at 360 nm for ML_2 is more intense than the peak at 313 nm (Fig. 6c). In the case of the Fe^{2+}-L system, Fe^{2+} does not absorb at wavelengths higher than 400 nm. The variations of the stoichiometries of the complexes can be seen in the concentration profiles in Fig. 6. As can be seen in Figs. 6a,a′, with a mole ratio of 0.5, the concentration of ML_2 complex starts to decrease. However, as can be seen in Figs. 6b, b′, with a mole ratio of 1.0, the concentration of ML starts to decrease. The stoichiometries of 1:1 and 1:2 for the complex formation of Fe^{2+} and Fe^{3+} with ligands, such as the ligand in this study, were previously reported [48–51].

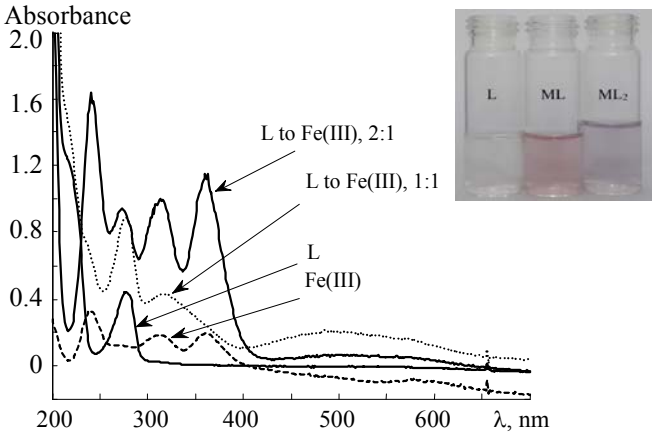

Fig. 7. Spectra of the solutions L (100.0 μmol/L) in mole ratio (L to Fe^{3+}) of 1:1 (pink) and 2:1 (purple). Inset shows the color changes of the solutions.

Color changes during the addition of Fe^{3+} to a solution of L are shown in Fig. 7. In the case of the 1:1 mole ratio, the color is pink, and for the 2:1 and 3:1 mole ratios, the color changes to purple. The spectra of these colored solutions are shown in Fig. 7. As can be seen, these spectra are in close agreement with the calculated spectral profiles shown in Fig. 6c.

Conclusion. Multidentate compounds have the ability to form selective stable complexes with metal ions with compatible dimensions and can potentially be used in their separation and determination. The multidentate ligand synthesized here can be used as a selective sensor for the simultaneous determination of Fe^{2+} and Fe^{3+} in environmental, agricultural, and medicinal analysis. It should be mentioned that the discrimination between Fe^{2+} and Fe^{3+} is very important in order to understand the biological functions regulated by iron. Moreover, it was shown that HM is able to elucidate different complex species in complex formation systems. With HM, it is possible to calculate the profiles of the components of the system, and it is a robust method for the determination of the stoichiometry of complexes.

REFERENCES

1. A. P. D. Silva, H. Q. N. Gunaratne, T. Gunnlaugsson, A. J. M. Huxley, C. P. McCoy, J. T. Rademacher, *Chem. Rev.*, **97**, 1515 (1997).
2. W. T. Mason, *Fluorescent and Luminescent Probes for Biological Activity*, Academic Press, San Diego (1999).
3. S. R. Liu, S. P. Wu, *Sens. Actuators B*, **171**, 1110 (2012).
4. Z. J. Jiang, H. S. Lv, J. Zhu, B. X. Zhao, *Synth. Met.*, **162**, 2112 (2012).
5. R. Azadbakht, H. Keypour, H. Amiri Rudbari, A. H. Mohammad Zaheri, S. Menati, *J. Lumin.*, **132**, 1860 (2012).
6. X. Wang, W. Zheng, H. Lin, G. Liu, Y. Chen, Y. Fang, *J. Tetrahedron Lett*., **50**, 1536 (2009).
7. P. S. Hariharan, N. Hari, S. P. Anthony, *Inorg. Chem. Commun*., **48**, 1 (2014).
8. Y. Liu, E.-B. Yang, R. Han, D. Zhang, Y. Ye, Y.-F. Zhao, *Chin. Chem. Lett*., **25**, 1065 (2014).
9. R. Azadbakht, T. Almasi, H. Keypour, M. Rezaeivala, *Inorg. Chem. Commun*., **33**, 63 (2013).
10. C. Y. Li, Y. Zhoua, Y. F. Li, X. F. Kong, C. X. Zou, C. Weng, *Anal. Chim. Acta*, **774**, 79 (2013).
11. R. Martínez-Máñez, F. Sancenón, *Coord. Chem. Rev*., **250**, 3081 (2006).
12. M. Vazquez, L. Fabbrizzi, A. Taglietti, R. M. Pedrido, A. M. Gonzalez-Noya, M. R. Bermejo, *Angew. Chem. Int. Ed.*, **44**, 1962 (2004).
13. J. V. Ros-Lis, R. Martínez-Máñez, Soto, *J. Org. Lett*., **7**, 2337 (2005).
14. T. Gunnlaugsson, M. Glynn, G. M. Tocci, P. E. Kruger, F. M. Pfeffer, *Coord. Chem. Rev.*, **250**, 3094 (2006).
15. G. Sivaraman, V. Sathiyaraja, D. Chellappa, *J. Lumin*., **145**, 480 (2014).
16. M. W. Henze, M. U. Muckenthaler, B. Galy, C. Camaschella, *Cell*, **142**, 24 (2010).

17. X. F. Liu, E. C. Theil, *Acc. Chem. Res*., **38**, 167 (2005).
18. C. A. Perez, Y. Tong, M. Guo, *Cur. Bioact. Compd*., **4**, 150 (2008).
19. M. José Casanueva Marenco, C. Fowley, B. W. Hyland, G. R.C. Hamilton, D. Galindo-Riaño, J. F. Callan, *Tetrahedron Lett*., **53**, 670 (2012).
20. A. F. Oliverra, J. A. Nobrega, O. Fatibello-Filho, *Talanta*, **49**, 505 (1995).
21. W. Qin, Z. J. Zhang, F. C. Wang, *Fresenius J. Anal. Chem*., **360**, 130 (1998).
22. J. M. T.Carneiro, A. C. B. Dias, E. A. G. Zagatto, R.S. Honorato, *Anal. Chim. Acta*, **455**, 327 (2002).
23. A. Safavi, H. Abdollahi, M. R. Hormozi-Nezhad, *Talanta*, **56**, 699 (2002).
24. B. M. Nagabhushana, G. T. Chandrappa, B. Nagappa, N. H. Nagaraj, *Anal. Bioanal. Chem.*, **373**, 299 (2002).
25. J. Zolgharnein, H. Abdollahi, D. Jaefarifar, G. H. Azimi, *Talanta*, **57**, 1067 (2002).
26. L. Donga, C. Wu, X. Zeng, L. Mu, S. F. Xue, Z. Tao, J. X. Zhang, *Sens. Actuators B*, **145**, 433 (2010).
27. E. M. Nolan, S. J. Lippard, *Acc. Chem. Res*., **42**, 193 (2009).
28. S. J. Lippard, J. M. Berg, *Principles of Bioinorganic Chemistry*, University Science Book, Mill Valley, CA, 10, 14, 78–183 (1994).
29. B. L. Vallee, K. H. Falchuk, *Physiol. Rev*., **73**, 79 (1993).
30. J. J. R. F. de Silva, R. J. P. Williams, *The Biological Chemistry of Elements: the Inorganic Chemistry of Life*, 2nd ed., Oxford University Press, New York (2001).
31. A. I. Bush, W. H. Pettingell, G. Multhaup, M. Paradis, J. P. Vonsattel, J. F. Gusella, K. Beyreuther, C. L. Masters, R.E. Tanzi, *Science*, **265**, 1464 (1994).
32. J. Y. Koh, S. W. Suh, B. J. Gwag, Y. Y. He, C. Y. Hsu, D.W. Choi, *Science*, **272**, 1013 (1996).
33. C. F. Walker, R. E. Black, *Annu. Rev. Nutr*., **24**, 255 (2004).
34. E. M. Nolan, S. J. Lippard, *Inorg. Chem*., **43**, 8310 (2004).
35. E. M. Nolan, S. C. Burdette, J. H. Hervey, S. A. Hilderbrand, S. J. Lippard, *Inorg. Chem*., **43**, 2624 (2004).
36. S. Aoki, D. Kagata, M. Shiro, K. Takeda, E. Kimura, *J. Am. Chem. Soc*., **126**, 13377 (2004).
37. R. Parkesh, T. C. Lee, T. Gunnlaugsson, *Org. Biomol. Chem*., **5**, 310 (2007).
38. M. Maeder, Y.-M. Neuhold, *Practical Data Analysis in Chemistry*, Elsevier, Amsterdam (2007).
39. M. Maeder, H. Abdollahi, *J. Iran. Chem. Soc*., **5**, 522 (2008).
40. H. S. Jung, P. S. Kwon, J. W. Lee, J. I. Kim, C. S. Hong, J. W. Kim, S. Yan, J. Y. Lee, J. H. Lee, T. Joo, J. S. Kim, *Chem. Soc*., **131**, 2008 (2009).
41. G. E. Malashkevich, M. V. Korzhik, M. G. Livshits, V. B. Pavlenko, A. L. Blinov, M. A. Borik, *The Sov. J. Glass Phys. Chem*., **15**, 397 (1990).
42. J. P. Sumner, R. Kopelman, *Analyst*, **130**, 528 (2005).
43. Y. Ma, W. Luo, P. J. Quinn, Z. Liu, R. C. Hider, *J. Med. Chem*., **47**, 6349 (2004).
44. J. M. Liu, Q. Y. Zheng, J. L. Yang, C. F. Chen, Z. T. Huang, *Tetrahedron Lett*., **43**, 9209 (2002).
45. G. Puxty, M. Maeder, K. Hungerbühler, *Chemom. Intell. Lab. Syst*., **81**, 149 (2006).
46. N. McCann, M. Maeder, *Anal. Chim. Acta*, **647**, 31 (2009).
47. M. Shariati-Rad, M. Hasani, *Anal. Chim. Acta*, **648**, 60 (2009).
48. Y. W. Choi, G. J. Park, Y. J. Na, H. Y. Jo, S. A. Lee, G. R. You, C. Kim, *Sens. Actuators B*, **194**, 343 (2014).
49. W. Zhu, L. Yang, M. Fang, Z. Wu, Q. Zhang, F. Yin, Q. Huang, C. Li, *J. Lumin*., **158**, 38 (2015).
50. S. Devaraj, Y. K. Tsui, C. Y. Chiang, Y. P. Yen, *Spectrochim. Acta A*, **96**, 594 (2012).
51. L. Wang, H. Li, D. Cao, *Sens. Actuators B*, **181**, 749 (2013).